Activation of cortical somatostatin interneurons prevents the development of neuropathic pain

Joseph Cichon[1,2,3], **Thomas JJ Blanck**[4], **Wen-Biao Gan**[1,2], and **Guang Yang**[2,4]

[1]Skirball Institute of Biomolecular Medicine, Department of Neuroscience and Physiology, New York University School of Medicine, New York, New York, USA

[2]Neuroscience Institute, New York University School of Medicine, New York, New York, USA

[3]Medical Scientist Training Program at New York University School of Medicine, New York, New York, USA

[4]Department of Anesthesiology, Perioperative Care and Pain Medicine, New York University School of Medicine, New York, New York, USA

Abstract

Neuropathic pain involves long-lasting modifications of pain pathways that result in abnormal cortical activity. How cortical circuits are altered and contribute to the intense sensation associated with allodynia is unclear. Here we report a persistent elevation of layer V pyramidal neuron activity in the somatosensory cortex of a mouse model of neuropathic pain. This enhanced pyramidal neuron activity was caused in part by increases of synaptic activity and NMDA-receptor-dependent calcium spikes in apical tuft dendrites. Furthermore, local inhibitory interneuron networks shifted their activity in favor of pyramidal neuron hyperactivity: somatostatin-expressing and parvalbumin-expressing inhibitory neurons reduced their activity, whereas vasoactive intestinal polypeptide–expressing interneurons increased their activity. Pharmacogenetic activation of somatostatin-expressing cells reduced pyramidal neuron hyperactivity and reversed mechanical allodynia. These findings reveal cortical circuit changes that arise during the development of neuropathic pain and identify the activation of specific cortical interneurons as therapeutic targets for chronic pain treatment.

Introduction

Neuropathic pain is a chronic pain state resulting from peripheral and/or central nerve injury[1]. The development of persistent pain is believed to be due to the long-lasting changes of neuronal functions in the pain transmission pathway, from peripheral nociceptors and the spinal cord to supraspinal and cortical areas including the primary somatosensory cortex

Correspondence should be addressed to G.Y. (guang.yang@med.nyu.edu).

(S1) and the anterior cingulate cortex (ACC)[2-6]. The S1 is an important cortical area responsible for the sensory aspects of the pain, such as the intensity and location of the pain[7, 8]. This cortical region is consistently activated during nociception and becomes hyperactive under chronic pain states. In both human and animal studies, the S1 of nerve-injured subjects shows increased activation, somatotopic reorganization, and changes in cortical thickness[9-11]. Furthermore, strategies to reduce S1 hyperexcitability and reorganization demonstrate benefits against chronic pain development[12-14].

How neuronal circuitry in the S1 is modified and becomes hyperactive during the development of neuropathic pain remains unclear. At the cellular level, the chronic pain states have been associated with structural and functional alterations in cortical pyramidal neurons, including long-term potentiation of synaptic transmission, new dendritic spine formation, increases in intrinsic cellular excitability, and rearrangements in ion channels[15-20]. In addition to these changes in glutamatergic pyramidal neurons, alterations of a highly interconnected network of GABAergic interneurons may also contribute to the persistent pain state. For example, increased activities of both excitatory neurons and local interneurons in layer II/III (L2/3) of the S1 were observed in a model of inflammatory pain[21]. Within the S1, there is a large diversity of cortical interneurons including parvalbumin (PV), somatostatin (SOM) and vasoactive intestinal polypeptide (VIP)-expressing neurons[22]. These different types of interneurons target specific domains of the principal neurons or other interneurons, providing precise spatiotemporal control of excitatory/inhibitory outputs and cortical dynamics. How changes in glutamatergic pyramidal neurons and interneuron populations contribute to the hyperactivity in the S1 and the intense sensation in neuropathic pain are unknown.

In this study, we investigated changes of layer V (L5) pyramidal neurons and three interneuron types in the S1 following spared nerve injury (SNI), a model for neuropathic pain in mice[23, 24]. By imaging and manipulating neuronal activity in living mice, we identified cell-type specific changes in the S1 that were important for the development of neuropathic pain. Our results also suggest modulating interneuron activity as an effective strategy for correcting pyramidal neuron hyperactivity and mitigating mechanical allodynia.

Results

Peripheral nerve injury causes pyramidal neuron hyperactivity in the S1

To identify cortical changes related to neuropathic pain, we used *in vivo* two-photon calcium (Ca^{2+}) imaging to examine somatic activities of pyramidal neurons expressing a genetically-encoded Ca^{2+} indicator (GCaMP6s) in the S1 of awake, head-restrained mice. To induce persistent neuropathic pain, mice were subjected to SNI (see materials and methods)[23, 24] (Fig. 1a). Two days after SNI, mice experienced mechanical allodynia in the injured hind paw, as revealed by a marked reduction in the paw withdrawal threshold upon pressure application to the lateral aspect of the plantar paw surface by a von Frey filament (Fig. 1b). This mechanical hypersensitivity persisted for more than 1 month. In contrast, sham-operated mice (Sham) did not exhibit pain behavior when assessed after 1 week. Both SNI and Sham showed no changes in paw withdrawal threshold in the intact limbs.

We first examined the activities of L5 pyramidal neurons, the major output cells in the S1 that integrate sensory inputs from thalamic and intracortical origin[25]. In the region of the S1 corresponding to the injured hind limbs of the animals, we found that Ca^{2+} activities in the somata of L5 pyramidal neurons (located > 600 μm below the pial surface) were about 3-fold higher in SNI mice in a quiet resting state than in Sham mice at 1 month post-surgery (Fig. 1c-e). In SNI mice, the elevation of L5 neuron somatic Ca^{2+} activity occurred in the S1 contralateral to the surgical site, but not in the ipsilateral S1 (Fig. 1d), and the degree of hyperactivity highly correlated with the severity of mechanical allodynia (Fig. 1e). L5 hyperactivity was observed at 1 week post-SNI when chronic pain behavior was apparent, and lasted for at least 2 months (Supplementary Fig. 1). Moreover, intraperitoneal injection of MK801, an antagonist of N-methyl-D-aspartate (NMDA) receptors, reduced the level of L5 Ca^{2+} activity in SNI mice to that in Sham mice at 1 week and 1 month (Supplementary Fig. 1), suggesting the involvement of NMDA receptor activity in the hyperactivity of L5 pyramidal neurons after SNI. Notably, at 2 weeks post-surgery, inhibiting peripheral sensory inputs by local administration of sodium channel blocker tetrodotoxin (TTX, 100 nM) to sciatic nerve reduced the level of L5 somatic Ca^{2+} activity in the S1 of Sham, but not SNI mice (Fig. 1f), suggesting that L5 hyperactivity was not driven solely by the peripheral inputs after the development of neuropathic pain.

In addition to hyperactivity of L5 pyramidal neurons, we found that the somata of layer II/III (L2/3) pyramidal neurons (located 200–300 μm below the pial surface) also exhibited higher levels of Ca^{2+} activity in SNI mice as compared to Sham (Supplementary Fig. 2). As in L5 neurons, this elevated neuronal activity could be observed shortly after SNI, at 1 week, and was sustained over 2 months (Supplementary Fig. 2). Together, these findings indicate that peripheral nerve injury causes a robust and persistent hyperactivity of pyramidal neurons in the S1.

Increased dendritic spine and branch activity in mice with neuropathic pain

The increased activity of L5 pyramidal neurons associated with neuropathic pain could be due to either an increase of excitatory drive onto these neurons, a reduction of inhibition, enhanced intrinsic excitability, or any combinations of these. To examine whether the excitatory inputs onto L5 pyramidal neurons increase in neuropathic pain, we imaged and measured Ca^{2+} activity on the apical tuft branches (10–100 μm below pial surface) of L5 pyramidal neurons (Fig. 2). Ca^{2+} activity in dendritic spines of L5 pyramidal neurons was readily observed in both SNI and Sham mice. Notably, we found that SNI mice showed a marked increase in dendritic spine Ca^{2+} activity as compared to Sham mice (Fig. 2a-d). Furthermore, spine pairs randomly selected from individual dendritic branches displayed greater coactivity in SNI mice than in sham mice (Fig. 2e-f).

In addition to localized Ca^{2+} activity in spines, we also observed Ca^{2+} transients generating across long segments (>30 μm) of L5 apical tuft dendrites. These dendritic Ca^{2+} transients occurred across long stretches of dendrites with comparable F/F_0, and lasted several seconds (Fig. 2a,g). They were similar to dendritic Ca^{2+} spikes observed in pyramidal neurons in other cortical regions of living animals[26, 27]. When comparing SNI to Sham, we found that dendritic Ca^{2+} spikes occurred more frequently in SNI mice (Fig. 2a,h).

Furthermore, the average peak amplitude (Fig. 2i) and average total integrated activity (Fig. 2j) of these dendritic Ca^{2+} spikes were also higher in SNI mice than in Sham mice.

Like the somatic activity, enhanced tuft Ca^{2+} activity of L5 pyramidal neurons persisted from 1 week to 2 months (Supplementary Fig. 3). These dendritic Ca^{2+} spikes were substantially reduced in the presence of locally delivered MK801 or TTX in layer 1 (L1) (Fig. 2j). We also found that spines on dendritic branches with more frequent dendritic Ca^{2+} spikes showed more coactivity in both SNI and Sham mice (Fig. 2f). Together, these observations reveal enhanced and synchronized dendritic spine activity and the generation of NMDA receptor-dependent Ca^{2+} spikes across apical tuft branches of L5 pyramidal neurons in the S1 of SNI mice, suggesting that the excitatory drive onto L5 pyramidal neurons increases after the development of neuropathic pain.

Apical tuft Ca^{2+} transients contribute to L5 pyramidal cell hyperactivity

Previous studies have shown that apical tuft dendrites exhibit Ca^{2+} spikes in either entire or a subset of branches in various cortical regions[26, 27]. These dendritic Ca^{2+} spikes substantially boost the firing of L5 pyramidal neurons[26, 28]. To better understand the contribution of apical tuft activity to the hyperactivity of L5 pyramidal neurons, we performed Ca^{2+} imaging at different cortical depths from the pial surface. In higher-order tuft branches converging toward the nexus (primary branch point from the apical trunk, located 150–250 μm from the pial surface), we observed elevated dendritic Ca^{2+} activity on multiple sibling branches of L5 pyramidal neurons (Fig. 3a). At this cortical depth, the majority of Ca^{2+} transients (Sham, $58 \pm 4.1\%$; SNI, $67 \pm 6.2\%$) occurred simultaneously in all branches (global) of the same L5 pyramidal neuron (Fig. 3b). At the apical trunk nexus of L5 pyramidal neurons, located 250–350 μm below the pial surface, repetitive Ca^{2+} activity occurred in both SNI and Sham mice (Fig. 3c). The total integrated trunk Ca^{2+} activity was greater in SNI than in Sham mice at 1 month post-surgery (Fig. 3d).

We found that local application of MK801 to L1 reduced the apical trunk Ca^{2+} activity in both SNI and Sham mice (Fig. 3d). Furthermore, local application of TTX to L1 reduced Ca^{2+} activity in both trunks and somata of L5 pyramidal neurons in SNI mice (Fig. 3e), suggesting that the apical trunk and somatic hyperactivity in L5 pyramidal neurons depends on synaptic activities originating in L1. Collectively, these results indicate that following the induction of neuropathic pain, a substantial fraction of apical tuft dendrites of L5 pyramidal neurons in the S1 receive synchronized synaptic inputs and generate persistent, NMDA receptor-dependent Ca^{2+} spikes, which lead to the hyperactivity of L5 pyramidal neurons.

SOM and PV interneurons reduce activity while VIP cells increase activity in neuropathic pain

To further understand mechanisms underlying the hyperactivity of L5 pyramidal neurons in the S1, we examined the activities of local inhibitory cells during the development of neuropathic pain. Recent studies have shown that SOM-positive inhibitory interneurons are important in regulating dendritic and somatic activity of pyramidal neurons[27, 29-31]. To measure the impact of neuropathic pain on SOM cell responses, we used *in vivo* two-photon Ca^{2+} imaging to examine the activity of SOM cells expressing GCaMP6s following SNI/

Sham surgeries. In this experiment, SOM-*IRES*-Cre mice were injected with a Cre-dependent adeno-associated virus (AAV) to induce the expression of GCaMP6s specifically in SOM cells. In contrast to the increased activity of pyramidal neurons, we found that SOM cell activities were reduced by half (52%) at 1 month post-SNI (Fig. 4a-b and Supplementary Fig. 4). This reduction in SOM cell activity was also observed in their axon fibers projecting to L1 (Fig. 4c-d). Furthermore, SOM cells imaged at 1 week post-surgery showed a reduction in neuronal activity in SNI as compared to Sham mice (Supplementary Fig. 4). These *in vivo* Ca^{2+} recordings show that peripheral nerve injury induces a potent and persistent reduction in SOM cell firing rates in the S1.

In addition to SOM neurons, we also investigated whether PV-positive interneurons were affected by neuropathic pain using PV-*IRES*-Cre mice expressing GCaMP6s. We found that PV cells also displayed a significant reduction in neuronal activity in SNI mice as compared to Sham mice at 1 week and 1 month post-surgery (Fig. 4e-f and Supplementary Fig. 5). The reduction (~30%) in PV cell activity at 1 month was not as robust as that of SOM cells (~50%) when comparing SNI to Sham mice. Because SOM and PV neurons target different regions of pyramidal cells (tuft dendrites versus perisomatic region), reduced activity from these cells suggests a lack of inhibitory tone across the somatodendritic axis of pyramidal neurons to promote pyramidal cell hyperactivity in neuropathic pain.

In addition to SOM and PV, VIP-expressing interneurons constitute another major subtype of neocortical interneurons, and are known to directly inhibit the activity of both SOM- and PV-expressing interneurons *in vitro* and *in vivo*. This connectivity scheme of VIP→SOM/PV →pyramidal cells is thought to amplify and modulate local neuronal activities[32]. To determine whether VIP neurons might be involved in the alterations of SOM and PV cell activity in neuropathic pain, we infected VIP-*IRES*-Cre mice with AAV virus encoding GCaMP6s and imaged Ca^{2+} activity of VIP neurons in SNI and Sham mice. Consistent with the disinhibition hypothesis, we found ~90% increase in the activities of VIP neurons in SNI as compared to Sham at 1 month post-surgery (Fig. 4g-h). The increased VIP neuron activity was also observed at 1 week post-SNI as compared to the Sham control (Supplementary Fig. 5). Taken together, these experiments indicate that the development of neuropathic pain is accompanied by distinct and persistent changes of neuronal activity in different types of interneurons including reduced neuronal activities of SOM and PV cells and an activation of VIP-expressing cells (see model in Supplementary Fig. 5).

Transient activation of SOM interneurons dampens L5 pyramidal cell hyperactivity in neuropathic pain

Previous studies have shown that SOM cells regulate branch-specific Ca^{2+} spike generation *in vivo* and control electrical and biochemical signaling in dendritic spines[27, 29, 30]. To test whether the reduction of SOM cell activity in SNI mice contributes significantly to the hyperactivity of L5 pyramidal neurons, we activated SOM cells under the neuropathic pain condition. To increase SOM cell activity *in vivo*, we specifically infected SOM cells of S1 with an AAV encoding Cre-dependent hM_3Dq DREADD receptors in SOM-Cre mice (Supplementary Fig. 6)[33]. Binding of the ligand clozapine N-oxide (CNO) to hM_3Dq receptors activates G*q*-coupled signaling, leading to membrane depolarization through

inhibition of KCNQ channels, which increases neuronal firing in target cells. Indeed, CNO delivered by intraperitoneal injection to mice expressing hM$_3$Dq specifically in SOM cells induced a more than threefold increase in SOM somatic Ca^{2+} activity *in vivo* in both SNI and Sham mice (Fig. 5a-b). To determine the effect of transient activation of SOM cells on pyramidal neuron activity in neuropathic pain, we imaged GCaMP6s-expressing L5 pyramidal neurons in mice expressing hM$_3$Dq in SOM cells. Ca^{2+} activities in dendrites and somata of L5 pyramidal neurons were measured before and 20 min after CNO injection. In both SNI and Sham, we found that acute activation of SOM cells induced a reduction in total integrated Ca^{2+} activity of both apical tuft dendrites and somata of L5 pyramidal neurons (Fig. 5c-f). Moreover, the somatic Ca^{2+} activity of L2/3 pyramidal neurons was also decreased after acute SOM activation with CNO (Supplementary Fig. 7). In contrast to the reduction in L5 neuron activity induced by SOM-hM$_3$Dq, inactivating SOM cells with the inhibitory DREADD variant (G$_i$-coupled hM$_4$Di) exacerbated Ca^{2+} activity of L5 dendrites and somata in SNI and Sham mice (Fig. 5g-i). As a control, we infected SOM-Cre mice with a control AAV vector (TurboRFP). As expected, administration of CNO to mice that did not express hM3D*q* receptors had no effect on L5 pyramidal neuron activity (Supplementary Fig. 8).

When mechanical hypersensitivity in SOM-Cre mice infected with AAV-hM$_3$Dq was tested (Fig. 5j), we found that acute activation of SOM cells with a single injection of CNO significantly increased the plantar pressure required to elicit paw withdrawal in SNI mice, whereas CNO injection in Sham exerted no effects on the animals' behavior (Fig. 5k). SNI/Sham mice infected with AAV-*CMV*-TurboRFP showed no changes in pain threshold after receiving a CNO injection (Supplementary Fig. 8). Furthermore, unlike the substantial reduction (52%) of SOM activity and reduced paw withdrawal threshold in SNI mice, we found that a milder reduction (25%) of SOM cell activity with AAV-hM$_4$Di/CNO in naïve mice had no effect on the animals' paw withdrawal threshold (Fig. 5l). Taken together, these findings indicate that acute activation of SOM cells in the S1 is sufficient to reduce pyramidal cell activity and improve mechanical allodynia in neuropathic pain.

In contrast to its effect on the activity of SOM cells, CNO treatment had milder effect (less than a twofold increase) on the neuronal activity of PV cells expressing hM$_3$Dq in both SNI and Sham mice (Fig. 5m and Supplementary Fig. 9). When withdrawal threshold in PV-Cre mice infected with AAV-hM$_3$Dq was tested, CNO injection had no effects on the animals' pain sensation in either SNI or sham mice (Fig. 5n), suggesting that increasing PV cell activity with the DREADD-CNO approach is less effective at alleviating mechanical allodynia than increasing SOM cell activity.

Continuous SOM cell activation prevents the development of mechanical allodynia

The results above highlight the immediate beneficial effects of SOM interneuron activation in neuropathic pain at the cellular and behavioral level. However, it remains unknown whether continuous activation of SOM cells might preclude the establishment of mechanical allodynia. To test this possibility, following the SNI/Sham surgery in mice expressing hM$_3$Dq in SOM cells, we performed daily CNO injections for 1 week and imaged Ca^{2+} activity in L5 pyramidal neurons 1 day after the last CNO treatment (Fig. 6a). Consistent

with previous reports[34], a single injection of CNO activated SOM cells over a period of ~12 h (Fig. 6b). We found that daily CNO treatment for 1 week was sufficient to prevent SNI-induced pyramidal neuron hyperactivity (Fig. 6c-d). At the level of apical tuft dendrites, we found no significant difference in the average Ca^{2+} activity between SNI and Sham mice (Fig. 6e-f). Moreover, we found no significant difference in the frequency of dendritic Ca^{2+} spikes between SNI and Sham mice ($P = 0.63$; Sham daily CNO: 2.4 ± 0.35 events per active dendrite in 2.5 min; SNI daily CNO: 2.6 ± 0.39 events per active dendrite in 2.5 min). These results indicate that chronic activation of SOM cells in the S1 with daily CNO treatment reduces the dendritic and somatic Ca^{2+} activity of L5 pyramidal neurons.

Notably, when paw withdrawal threshold was measured over time (Fig. 6a), we found that SOM cell activation for 1 week mitigated the mechanical allodynia in SNI mice as compared to saline-treated controls (Fig. 6g). One to three weeks after the last CNO injection at day 7, the pain threshold of SNI mice was not significantly different from that of Sham mice, indicating that continuous activation of SOM cells with daily CNO treatment for 1 week prevents the formation of persistent pain in SNI mice.

Discussion

While considerable efforts have been made towards unraveling the maladaptive changes in the spinal cord after peripheral nerve damage, much less is known about how cortical circuits are reorganized in chronic pain conditions. Using *in vivo* two-photon Ca^{2+} imaging, we found that pyramidal neurons located in L2/3 and L5 of S1 were hyperactive in a mouse model of neuropathic pain. We further found that increased synaptic inputs, dendritic Ca^{2+} spike generation, and changes of the activity of three major populations of cortical GABAergic interneurons collectively promoted pyramidal neuron hyperactivity (Supplementary Fig. 10). In addition, continuous activation of SOM-expressing interneurons suppressed the hyperactivity of pyramidal neurons and mechanical allodynia over 1 month. These findings indicate that dysfunctional inhibitory circuits contribute substantially to the hyperactivity of pyramidal neurons during neuropathic pain development and suggest that manipulation of interneuron activity could be an effective strategy for treating chronic pain.

Pyramidal neuron hyperactivity in neuropathic pain

Both L2/3 and L5 pyramidal neurons in the S1 become profoundly activated after peripheral nerve injury (Fig. 1 and Supplementary Figs. 1 and 2)[16]. When considering ascending sensory information flow through the S1, L2/3 neurons are classically positioned upstream of L5 neurons: the information flows from thalamic inputs to L4 neurons, from L4 to L2/3, and then from L2/3 to L5. However, recently it has been shown that thalamus can directly activate deep cortical layers[35]. Therefore, both L2/3 and L5 neurons of S1 can be activated by ascending sensory information from the thalamus, and both layers eventually transmit information out of the S1 to the other brain areas associated with the processing of pain information, including subcortical regions for descending pain modulation[26]. Future use of genetic approaches to manipulate neurons in specific cortical layers will aid in further delineating the contribution of L2/3 versus L5 neurons to the development of neuropathic pain.

One noteworthy finding of the current study is that the increased spontaneous activity of L5 pyramidal neurons in the S1 is not reduced by acute silencing of peripheral sciatic nerves at 2 weeks post-SNI (Fig. 1f). These results suggest that peripheral nerve discharges are not the sole component driving the abnormal cortical activity after the development of the chronic pain. Previous studies have demonstrated a relief of spontaneous pain by systemic or spinal analgesia in animal models of neuropathic pain[36, 37]. Future study will be needed to better understand to what degree the maintenance of S1 hyperactivity in chronic pain condition requires the inputs from the peripheral or spinal inputs.

Dendritic Ca^{2+} spike generation in neuropathic pain

By imaging apical tuft dendrites of L5 pyramidal neurons, we found a substantial and persistent increase in dendritic spine Ca^{2+} activity and NMDA-receptor dependent dendritic Ca^{2+} spikes after peripheral nerve injury. Blockade of synaptic and dendritic activity in L1 of the S1 reduced L5 pyramidal neuron hyperactivity. These results suggest that elevated synaptic inputs and the persistence of Ca^{2+} spike generation are likely to play a critical role in maintaining the hyperactive state of L5 cells and potentially L2/3 cells in neuropathic pain. It has been shown that the development of neuropathic pain is associated with long-term potentiation of synaptic transmission in ACC[17], a brain region mediating affective responses to painful stimuli. Dendritic Ca^{2+} spikes have been shown to induce long-lasting changes in synaptic plasticity (long-term potentiation and long-term depression) of existing synapses[27, 38, 39]. It is thus possible that following SNI, the generation of dendritic Ca^{2+} spikes may play a role in synaptic potentiation and lead to the increased Ca^{2+} activity of dendritic spines in the S1. Dendritic Ca^{2+} spikes may also amplify synaptic inputs and increase the output of pyramidal neurons in SNI mice[28, 40]. Additionally, local Ca^{2+} spikes could potentially induce long-lasting changes by promoting formation of new dendritic spines[15], thus further contributing to persistent hyperactivity in the S1 after peripheral nerve injury.

The mechanisms underlying the elevated generation of dendritic Ca^{2+} spikes in apical tuft dendrites remain to be determined. Our studies suggest that synaptic inputs to apical tuft dendrites are more synchronized in SNI mice as compared to Sham mice. Such changes of synaptic input patterns favor dendritic Ca^{2+} spike generation. Notably, work in the ACC shows that peripheral nerve injury does not induce NMDA receptor-dependent dendritic Ca^{2+} spikes in the apical tuft of L5 pyramidal neurons, but rather is capable of generating fast local sodium dendritic spikes[19]. L5 pyramidal neuron hyperexcitability in this brain region is linked to dysfunctional HCN channels in apical tuft dendrites. It would be worthwhile to investigate how such changes of intrinsic excitability contribute to the generation of dendritic Ca^{2+} spikes and hyperactivity of L5 pyramidal neurons in the S1. Moreover, as discussed below, reduced dendritic inhibition also promotes the generation of dendritic Ca^{2+} spikes and hyperactivity of L5 pyramidal neurons in the S1.

Impaired cortical inhibition in neuropathic pain

Increasing evidence suggests that disinhibition of pain pathway is important to the development and maintenance of chronic pain. In the spinal cord, a loss of inhibitory neurotransmission has been implicated in several forms of chronic pain[41, 42]. Recent work in

the ACC suggests that the loss of inhibitory synapses onto excitatory pyramidal neurons and the loss of the excitatory drive onto inhibitory fast-spiking interneurons creates a disinhibited cortical network[18]. In the S1, peripheral nerve injury causes an overall increase in the activity of GABAergic interneurons that is ineffective in dampening excitatory neuron activity due to changes in KCC2 expression[21]. However, it is unknown whether different types of GABAergic interneurons may exhibit different changes in activity following peripheral nerve injury. In this study, we used two-photon Ca^{2+} imaging to examine the activities of three groups of cortical interneurons in the S1 of the awake mice. We found that peripheral nerve injury causes cell-type specific changes in the S1, in which VIP cells are activated; SOM and PV cell activities are downregulated. These changes developed within 1 week following peripheral nerve injury and persisted for more than 1 month. Previous studies have shown that three major subtypes of interneurons are connected in such a way that (1) VIP cells preferentially inhibit SOM cells; (2) SOM cells strongly inhibit all other populations yet avoid inhibiting one another; (3) PV cells inhibit each other but poorly inhibit other populations[22, 32, 43, 44]. Our findings are consistent with these findings and suggest that the activity of inhibitory circuits is shifted (VIP↑→SOM/PV↓→pyramidal cells↑) to increase excitatory activity in the S1 during the development and maintenance of neuropathic pain (Supplementary Fig. 10). It would be interesting to test whether manipulating this inhibitory circuitry toward pyramidal cell hyperactivity would be sufficient to elicit pain behaviors in naïve mice.

In contrast to the effect of manipulating SOM cells, we found that activation of PV cells was ineffective in altering the mechanical threshold for pain. This difference could be related to that (1) PV cells primarily synapse perisomatically and have minimal regulation on dendritic Ca^{2+} spikes; (2) PV cells may provide brief inhibition on pyramidal cell somata[45], whereas SOM cells exhibit high levels of spontaneous activity to inhibit apical dendrites of pyramidal neurons[46]. It is important to note that besides for the three major subtypes of interneurons in the S1, other interneurons located in L1, which do not express SOM, PV, or VIP markers, are known to target apical tuft dendrites and their activation can suppress Ca^{2+} spike generation in L5 pyramidal neurons of the S1[47]. Future studies will be needed to examine whether L1 interneuron dysfunction is also involved in pyramidal neuron hyperactivity during the development of chronic pain.

Targeting inhibitory interneurons to modulate the development of chronic pain

Our study provides, to our knowledge, the first direct evidence that impaired SOM cell activity is involved in the development of neuropathic pain. Given the reduction of SOM neuronal activity in SNI mice, we acutely manipulated the activity of S1 SOM cells and demonstrated that SOM cell activation was sufficient to decrease L5 dendritic and somatic Ca^{2+} hyperactivity. Notably, daily activation of SOM cells following SNI diminished L5 pyramidal neuron hyperactivity at the subcellular and cellular levels, as well as reducing mechanical allodynia. Hence, our findings suggest that manipulating interneuron activity after peripheral nerve injury could be an important avenue for the prevention of pyramidal neuron over-excitation, and the transition from acute post-operative pain to chronic centralized pain.

Interneurons are becoming interestingly attractive for disease intervention via small molecule medications because of their profound impact on cortical circuit dynamics. For example, SOM cells express distinct receptors that have potent effects on neuronal network activity[48, 49]. Activation of SOM neuropeptide receptors has been proposed as one avenue for silencing neuronal networks in the face of epilepsy[50], which may be worth evaluating as a strategy to treat neuropathic pain states. Aside from medications, transcranial magnetic stimulation (TMS), a technique that uses high-intensity magnetic field and a brief electric current to create stimulation, was found to suppress apical tuft dendritic Ca^{2+} activity in L5 neurons[47]. The use of TMS has been applied to many neurological diseases, such as schizophrenia, pain, depression, and epilepsy, where interneuron dysfunction is thought to be a fundamental defect of the circuit. Whether or not TMS can be used to modulate activities of different interneuron classes (SOM or VIP cells) would be of great interest in developing new treatments for chronic pain.

Online Methods

Experimental animals

Transgenic mice expressing GCaMP6s in Layer V (L5) pyramidal neurons, Thy1-GCaMP6 slow founder line 1, were generated at New York University School of Medicine. AAV experiments were conducted with C57BL/6 (Charles River Laboratory), Thy1-Cre (Jackson Laboratory; Stock No: 006143), PV-IRES-Cre (Jackson Laboratory; Stock No: 008069), SST-IRES-Cre (Jackson Laboratory; Stock No: 013044), and VIP-IRES-Cre mice (Jackson Laboratory; Stock No: 010908). Mice were group-housed in temperature-controlled rooms on a 12-h light-dark cycle, and were randomly assigned to different treatment groups. One-to 3-month-old animals of both sexes were used for all the experiments. All mice were maintained at the New York University Old Public Health animal facility. Animal research was approved by Institutional Animal Care and Use Committee (IACUC).

Spared nerve injury and von Frey test

Spared nerve injury (SNI) of the sciatic nerve or sham operation (Sham) was performed on C57BL/6 adult mice (8–12 weeks)[24]. In brief, surgeries were performed under strict sterile conditions. Mice were deeply anesthetized and a small incision in the left thigh was made to expose the sciatic nerve and axotomy/ligation of the tibial and common peroneal nerves was performed leaving the sural nerve intact. Great care was taken to avoid any contact with or stretching of the intact sural nerve. Muscle and skin were closed in two layers. For Sham surgery, the sciatic nerve was exposed but not ligated or cut. Von Frey test was used to assess the onset and maintenance of mechanical allodynia over time. In all animal groups, mechanical threshold was examined using an Electronic von Frey anesthesiometer (IITC Inc., Life Science Instruments) that measures the precise minimum pressure at which paw withdrawal occurs. Specifically, a von Frey tip of suitable rigidity was attached to an electronic probe and used to apply an increasing pressure to the lateral plantar aspect (the sural nerve skin territory) of the hind paw. The anesthesiometer displays the pressure at which the mouse retracts from the von Frey tip. Three trials for paw withdrawal were recorded for each day tested and an average was reported. Von Frey test was performed

during the light cycle by the same researcher who was blinded to the surgery, genotypes, and treatments (CNO versus saline).

Surgical preparation for imaging awake, head-restrained mice

Dendritic and somatic imaging was carried out in awake, head restrained mice under a quiet resting state[27]. Surgery preparation for awake animal imaging includes attaching a head holder and creating a cranial window[51]. Specifically, mice were deeply anesthetized with an intraperitoneal injection of ketamine (100 mg/kg) and xylazine (15 mg/kg) or isoflurane. The mouse head was shaved and the skull surface was exposed with a midline scalp incision. The periosteum tissue over the skull surface was removed without damaging the temporal and occipital muscles. A head holder composed of two parallel micro-metal bars was attached to the animal's skull with glue (Loctite 495) to help restrain the animal's head and reduce motion-induced artifact during imaging. A small skull region (~0.2 mm in diameter) located over the primary somatosensory cortex (S1) on the basis of stereotaxic coordinates (0.5 mm posterior and 1.5 mm lateral to the bregma) was removed and a round glass coverslip (approximately the same size as the bone being removed) was glued to the skull. Dental acrylic cement was applied to surrounding area to secure metal bars with precaution not to cover the glass region with cement.

Upon awakening, mice with head mounts were habituated for three times (10 min each time) in a custom-built imaging platform to minimize potential stress effects of head restraining and imaging. In this device, the animal's head-mount was secured into metal blocks such that their head was fixed and perpendicular to the two-photon objective. The animal's body was allowed to rest against the bottom of the solid imaging plate. There was no instrumentation to either of the animal's hind limbs during imaging. Imaging experiments were started ~12–24 hours after window implantation and free from anesthetic effects.

Ca^{2+} imaging in dendrites and somata of L5 pyramidal neurons expressing GCaMP6s

Genetically-encoded Ca^{2+} indicator GCaMP6 slow (GCaMP6s) was used for Ca^{2+} imaging of L5 pyramidal somata, apical dendrites, dendritic spines as well as somata and axons of interneurons in the S1. We utilized Thy1-Cre and Thy1-GCaMP6s (founder line 1) for pyramidal neuron imaging and PV, SOM, VIP Cre lines for interneuron imaging. For Cre mice, GCaMP6s was expressed with recombinant adeno-associated virus under the CAG promoter [AAV, serotype 2/1; >2×10^{13} (GC/ml) titer; produced by the University of Pennsylvania Gene Therapy Program Vector Core]. To ensure better spread of AAV throughout the S1, about 0.1–0.2 μl AAV viruses were diluted 10× in artificial cerebrospinal fluid (ACSF) and injected (Picospritzer III; 15 p.s.i., 12 ms, 0.8 Hz) over 10–15 min into L2/3 or 5 of the S1 using a glass microelectrode around the coordinates of 0.5 mm posterior, 2 mm lateral to the bregma. In Thy1-GCaMP6s mice, the average total GCaMP6s signal during recordings was slightly lower than that of Thy1-Cre mice injected with AAV-GCaMP6s due to the relative amount of GCaMP[52].

Acute and chronic SOM cell activation was accomplished with Cre-dependent DREADD-hM3Dq under the human SYN promoter in SOM-IRES-Cre mice [AAV, serotype 2/1; ~10^{12} (GC/ml) titer; produced by UNC Vector Core]. For validation of SOM activation

(DREADD-hM$_3$Dq) or inactivation (DREADD-hM$_4$Di) in vivo (Fig. 5a,b,g), two viruses (AAV2/1-CAG-Flex-GCaMP6s and AAV2/1-HSYN-DIO-hM$_3$Dq-mcherry/AAV2/1-HSYN-DIO-hM$_4$Di-mcherry) were mixed at equal volumes and injected into the S1 of SOM-IRES-Cre mice, and SOM cell activity was imaged before and 20 min after CNO intraperitoneal injection. In experiments where SOM cells were activated and pyramidal cells were imaged (Figs. 5 and 6), AAV2/1-HSYN-DIO-hM$_3$Dq-mcherry was injected into SOM-IRES-Cre/Thy1-GCaMP6s mice. Similarly, in experiments where SOM cells were inactivated and pyramidal cells were imaged (Fig. 5h,i), AAV2/1-HSYN-DIO-hM$_4$Di-mcherry was injected into SOM-IRES-Cre/Thy1-GCaMP6s mice. As a control for DREADD expression, S1 was infected with AAV2/1-CMV-TurboRFP (produced by the University of Pennsylvania Gene Therapy Program Vector Core) (Supplementary Fig. 8).

To evaluate the expression patterns of GCaMP6 and DREADD-Gq, SOM mice were fixed with 4% paraformaldehyde, brain was sectioned at 200 μm thickness, and immunostained against GFP (Abcam, ab13970,1:300) and RFP (Rockland, 600-401-379S, reactive against mCherry, 1:300) (Supplementary Figs. 6 and 9). Confocal microscopy (Zeiss LSM 700 confocal microscope; 10× air objective, numerical aperture 0.3) revealed that the average number of SOM cells in L2/3 of the S1 infected with AAV2/1-HSYN-DIO-hM$_3$Dq-mcherry was 205 ± 28 cells per 1 mm^2 (Sham, 8 sections) and 194 ± 34 cells per 1 mm^2 (SNI, 9 sections) (Supplementary Fig. 6). The average number of SOM cells in L2/3 of the S1 infected with AAV2/1-FLEX-CAG-GCaMP6s was 235 ± 21 cells per 1 mm^2 (Sham, 12 sections) and 265 ± 21 cells per 1 mm^2 (SNI, 15 sections). PV mice infected with AAV2/1-HSYN-DIO-hM3Dq-mcherry in the S1 had a labelling density of 110 ± 24 cells per 1 mm^2 (Sham, 6 sections) and 149 ± 13 cells per 1 mm^2 (SNI, 7 sections) (Supplementary Fig. 9). SOM mice infected with AAV2/1-CMV-TurboRFP in S1 had expression restricted to S1. Dimensions of the infected area (Supplementary Fig. 8) were similar between SNI and sham mice.

Transgenic mice infected with AAV were prepared for head-fixation and imaging after 2 weeks of AAV expression. In vivo two-photon imaging was performed with an Olympus Fluoview 1000 two-photon system equipped with a Ti:Sapphire laser (MaiTai DeepSee, Spectra Physics) tuned to 920 nm. The average laser power on the sample was ~20–30 mW for imaging in the L1 of the cortex. All experiments were performed using a 25× objective immersed in an ACSF solution and with a 2× (soma) and 4× (dendrites) digital zoom. All images were acquired at frame rates of 2–10 Hz (2-μs pixel dwell time). Image acquisition was performed using FV10-ASW v.2.0 software and analyzed *post hoc* using NIH ImageJ software.

Data Analysis

During quiet resting, motion-related artifact (animal's respiratory rate and heart beat) was typically less than 2 μm as detected in our cortical measurements. Vertical movements were infrequent and minimized by habituation, two micro-metal bars attached to the animal's skull (described above) by dental acrylic, and a custom-built body platform. If the animal struggled in the body platform, imaging time points from those segments were excluded from quantification. All imaging stacks were registered using NIH ImageJ plugin StackReg.

L2/3 and L5 soma—

Comparing calcium traces to neuronal firing rates—GCaMP6s can produce large fluorescence transients (~20% F/F) even in response to single action potentials and individual spikes within a burst result in stepwise fluorescence increases[53]. However, when neuronal firing rates are high, it becomes difficult to resolve the number of action potentials due to long decay time constant of GCaMP6 fluorescence. We found that there is diversity in calcium traces of pyramidal cells in SNI and Sham mice, which likely reflects burst and non-burst firing of L5 neurons[54, 55]. Although it is difficult to report firing rates based on calcium responses within individual cells, several studies using two-photon imaging and patch-clamp electrophysiology have found a significant correlation between calcium signals and action potential generation in L2/3 neurons *in vivo*[40, 56]. In order to compare neuronal activity among different cells, we performed an integrated measurement of a cell's output activity over 2.5-min recording, termed total integrated calcium activity, as well as peak fluorescent signal. The total integrate calcium activity is the average of F/F over 2.5 min.

Tuft apical dendrites—At the depth of ~10 to 100 μm below the pial surface, dendrites with GCaMP6s expression were included for analysis. Dendritic Ca^{2+} spikes were defined as an increase in Ca^{2+} fluorescence observed in both dendritic spines and shaft over >30 μm of dendrite within the two-photon imaging focal plane[27]. Dendritic Ca^{2+} spikes were expressed using the peak F/F_0, where $F/F_0 = (F-F_0)/F_0 \times 100$, F_0 is the background-corrected fluorescence. Fluorescence background was measured from a region adjacent to the dendrite. Reported Ca^{2+} transients of spikes had amplitudes more than 3 times the standard deviation, which was on average 35% F/F for 6 sec. The majority of Ca^{2+} spikes were found to have a fluorescence increase of 100 to >1,000%. In addition to peak amplitude, the total integrated Ca^{2+} activity of dendrites was defined by the area under Ca^{2+} transients over 2.5 min.

Dendritic spines—In Figure 2, dendritic spine Ca^{2+} transients were defined as those with changes of fluorescence (F/F_0) >35% for GCaMP6s during 1-min imaging session. The threshold was more than 3 times the standard deviation of baseline fluorescence noise for GCaMP6s. Spine co-activity was assessed by applying Pearson correlation coefficients to the fluorescence signal of the spine head across the 1-min recordings from random spine pairs on dendritic segments.

Drugs

Local application of drugs—MK801 (M107, Sigma Aldrich) and TTX citrate (1069, Tocris) was applied to the surface of the S1 after removing a small bone flap (~200 μm in

diameter) adjacent to a thinned skull window. MK801 (100 μM) and TTX (100 nM) were dissolved directly in ACSF to final concentrations. The bone flap for drug delivery was made during awake head mounting and covered with a silicone elastomer such that it could be easily removed at the time of imaging. Because small molecules diffuse rapidly in the cortex, we estimated that the drug concentration was reduced ~10 times in the imaged cortical region, such that the final effective concentration would be ~10 μM and 10 nM for MK801 and TTX, respectively. As a control, we applied ACSF after removing a bone flap. In Figure 1f, TTX (100 nM) was locally delivered to the surgical site of sciatic nerve. In Supplementary Figure 1, MK801 (15 μg/ml in saline; 0.1 or 0.25 μg/g body weight) was delivered by intraperitoneal injection.

DREADD activation of SOM cells—DREADD activation was achieved in SOM-IRES-Cre mice where AAV2/1-HSYN-DIO-hM$_3$Dq-mcherry was injected into the S1 two weeks prior to the Ca^{2+} imaging. AAV-CMV-TurboRFP was used as a control AAV vector. Clozapine N-oxide (CNO, C0832, Sigma Aldrich) was dissolved in saline to a concentration of 0.5 mg/ml. In Figure 5, Ca^{2+} imaging of dendritic tufts/somata was performed during a quiet resting state without CNO. Twenty minutes after CNO was administrated by intraperitoneal injection to each mouse (0.3 ml/30 g body weight), the same cortical region was reimaged for second session (another 2.5-min recording). Mechanical threshold was also assessed before and 20 min after CNO injection. In Figure 6, CNO/saline was injected daily over the first week (a total of 7 injections) following SNI. Consecutive CNO injections were spaced 24 h apart and mechanical threshold was measured 1 h before each CNO injection (or 23 h after previous CNO injection). No more CNO injection was given after the first week. Ca^{2+} imaging of dendritic tufts/somata was performed at day 8.

Statistics

Summary data were presented as means ± s.e.m. No statistical methods were used to pre-determine sample sizes but our sample sizes are similar to those reported in previous publications[27]. Data distribution was assumed to be normal but this was not formally tested. The variance was similar between groups that were being statistically compared. Tests for differences between two populations were performed using unpaired or paired *t* test. Two-way ANOVA followed by Bonferroni's or Tukey's test was also used to compare significance between various groups. Significant levels were set at *P* 0.05. All statistical analyses were performed using the GraphPad Prism.

Data availability

The authors declare that the data supporting the findings of this study are available within the article and its supplementary information files.

Supplementary Material

Refer to Web version on PubMed Central for supplementary material.

References

1. Baron R. Mechanisms of disease: neuropathic pain--a clinical perspective. Nature clinical practice Neurology. 2006; 2:95–106.

2. Costigan M, Scholz J, Woolf CJ. Neuropathic pain: a maladaptive response of the nervous system to damage. Annu Rev Neurosci. 2009; 32:1–32. [PubMed: 19400724]

3. Basbaum AI, Bautista DM, Scherrer G, Julius D. Cellular and molecular mechanisms of pain. Cell. 2009; 139:267–284. [PubMed: 19837031]

4. Kuner R. Central mechanisms of pathological pain. Nat Med. 2010; 16:1258–1266. [PubMed: 20948531]

5. Saab CY. Pain-related changes in the brain: diagnostic and therapeutic potentials. Trends Neurosci. 2012; 35:629–637. [PubMed: 22763295]

6. Bushnell MC, Ceko M, Low LA. Cognitive and emotional control of pain and its disruption in chronic pain. Nat Rev Neurosci. 2013; 14:502–511. [PubMed: 23719569]

7. Bushnell MC, et al. Pain perception: Is there a role for primary somatosensory cortex? P Natl Acad Sci USA. 1999; 96:7705–7709.

8. Gross J, Schnitzler A, Timmermann L, Ploner M. Gamma oscillations in human primary somatosensory cortex reflect pain perception. Plos Biology. 2007; 5:1168–1173.

9. Seifert F, Maihofner C. Central mechanisms of experimental and chronic neuropathic pain: findings from functional imaging studies. Cell Mol Life Sci. 2009; 66:375–390. [PubMed: 18791842]

10. Peyron R, et al. An fMRI study of cortical representation of mechanical allodynia in patients with neuropathic pain. Neurology. 2004; 63:1838–1846. [PubMed: 15557499]

11. Seminowicz DA, et al. MRI structural brain changes associated with sensory and emotional function in a rat model of long-term neuropathic pain. Neuroimage. 2009; 47:1007–1014. [PubMed: 19497372]

12. Flor H, Denke C, Schaefer M, Grusser S. Effect of sensory discrimination training on cortical reorganisation and phantom limb pain. Lancet. 2001; 357:1763–1764. [PubMed: 11403816]

13. Lotze M, et al. Does use of a myoelectric prosthesis prevent cortical reorganization and phantom limb pain? Nat Neurosci. 1999; 2:501–502. [PubMed: 10448212]

14. De Ridder D, De Mulder G, Menovsky T, Sunaert S, Kovacs S. Electrical stimulation of auditory and somatosensory cortices for treatment of tinnitus and pain. Prog Brain Res. 2007; 166:377–388. [PubMed: 17956802]

15. Kim SK, Nabekura J. Rapid synaptic remodeling in the adult somatosensory cortex following peripheral nerve injury and its association with neuropathic pain. J Neurosci. 2011; 31:5477–5482. [PubMed: 21471384]

16. Eto K, et al. Inter-regional contribution of enhanced activity of the primary somatosensory cortex to the anterior cingulate cortex accelerates chronic pain behavior. J Neurosci. 2011; 31:7631–7636. [PubMed: 21613476]

17. Li XY, et al. Alleviating neuropathic pain hypersensitivity by inhibiting PKMzeta in the anterior cingulate cortex. Science. 2010; 330:1400–1404. [PubMed: 21127255]

18. Blom SM, Pfister JP, Santello M, Senn W, Nevian T. Nerve injury-induced neuropathic pain causes disinhibition of the anterior cingulate cortex. J Neurosci. 2014; 34:5754–5764. [PubMed: 24760836]

19. Santello M, Nevian T. Dysfunction of cortical dendritic integration in neuropathic pain reversed by serotoninergic neuromodulation. Neuron. 2015; 86:233–246. [PubMed: 25819610]

Author Manuscript Author Manuscript Author Manuscript Author Manuscript

20. Kim SK, et al. Cortical astrocytes rewire somatosensory cortical circuits for peripheral neuropathic pain. The Journal of clinical investigation. 2016; 126:1983–1997. [PubMed: 27064281]

21. Eto K, et al. Enhanced GABAergic activity in the mouse primary somatosensory cortex is insufficient to alleviate chronic pain behavior with reduced expression of neuronal potassium-chloride cotransporter. J Neurosci. 2012; 32:16552–16559. [PubMed: 23175811]

22. DeFelipe J, et al. New insights into the classification and nomenclature of cortical GABAergic interneurons. Nat Rev Neurosci. 2013; 14:202–216. [PubMed: 23385869]

23. Decosterd I, Woolf CJ. Spared nerve injury: an animal model of persistent peripheral neuropathic pain. Pain. 2000; 87:149–158. [PubMed: 10924808]

24. Bourquin AF, et al. Assessment and analysis of mechanical allodynia-like behavior induced by spared nerve injury (SNI) in the mouse. Pain. 2006; 122:14 e11–14. [PubMed: 16542774]

25. Harris KD, Mrsic-Flogel TD. Cortical connectivity and sensory coding. Nature. 2013; 503:51–58. [PubMed: 24201278]

26. Xu NL, et al. Nonlinear dendritic integration of sensory and motor input during an active sensing task. Nature. 2012; 492:247–251. [PubMed: 23143335]

27. Cichon J, Gan WB. Branch-specific dendritic Ca(2+) spikes cause persistent synaptic plasticity. Nature. 2015; 520:180–185. [PubMed: 25822789]

28. Larkum ME, Nevian T, Sandler M, Polsky A, Schiller J. Synaptic integration in tuft dendrites of layer 5 pyramidal neurons: a new unifying principle. Science. 2009; 325:756–760. [PubMed: 19661433]

29. Chiu CQ, et al. Compartmentalization of GABAergic inhibition by dendritic spines. Science. 2013; 340:759–762. [PubMed: 23661763]

30. Marlin JJ, Carter AG. GABA-A Receptor Inhibition of Local Calcium Signaling in Spines and Dendrites. The Journal of Neuroscience. 2014; 34:15898–15911. [PubMed: 25429132]

31. Munoz W, Tremblay R, Levenstein D, Rudy B. Layer-specific modulation of neocortical dendritic inhibition during active wakefulness. Science. 2017; 355:954–959. [PubMed: 28254942]

32. Pi HJ, et al. Cortical interneurons that specialize in disinhibitory control. Nature. 2013; 503:521–524. [PubMed: 24097352]

33. Urban DJ, Roth BL. DREADDs (designer receptors exclusively activated by designer drugs): chemogenetic tools with therapeutic utility. Annu Rev Pharmacol Toxicol. 2015; 55:399–417. [PubMed: 25292433]

34. Alexander GM, et al. Remote control of neuronal activity in transgenic mice expressing evolved G protein-coupled receptors. Neuron. 2009; 63:27–39. [PubMed: 19607790]

35. Constantinople CM, Bruno RM. Deep Cortical Layers Are Activated Directly by Thalamus. Science. 2013; 340:1591–1594. [PubMed: 23812718]

36. King T, et al. Unmasking the tonic-aversive state in neuropathic pain. Nat Neurosci. 2009; 12:1364–1366. [PubMed: 19783992]

37. Navratilova E, et al. Pain relief produces negative reinforcement through activation of mesolimbic reward-valuation circuitry. P Natl Acad Sci USA. 2012; 109:20709–20713.

38. Golding NL, Staff NP, Spruston N. Dendritic spikes as a mechanism for cooperative long-term potentiation. Nature. 2002; 418:326–331. [PubMed: 12124625]

39. Remy S, Spruston N. Dendritic spikes induce single-burst long-term potentiation. Proc Natl Acad Sci U S A. 2007; 104:17192–17197. [PubMed: 17940015]

40. Palmer LM, et al. NMDA spikes enhance action potential generation during sensory input. Nat Neurosci. 2014; 17:383–390. [PubMed: 24487231]

41. Knabl J, et al. Reversal of pathological pain through specific spinal GABA(A) receptor subtypes. Nature. 2008; 451:330–U336. [PubMed: 18202657]

42. Coull JAM, et al. Trans-synaptic shift in anion gradient in spinal lamina I neurons as a mechanism of neuropathic pain. Nature. 2003; 424:938–942. [PubMed: 12931188]

43. Pfeffer CK, Xue M, He M, Huang ZJ, Scanziani M. Inhibition of inhibition in visual cortex: the logic of connections between molecularly distinct interneurons. Nat Neurosci. 2013; 16:1068–1076. [PubMed: 23817549]

44. Fu Y, et al. A cortical circuit for gain control by behavioral state. Cell. 2014; 156:1139–1152. [PubMed: 24630718]

45. Beierlein M, Gibson JR, Connors BW. Two dynamically distinct inhibitory networks in layer 4 of the neocortex. J Neurophysiol. 2003; 90:2987–3000. [PubMed: 12815025]

46. Urban-Ciecko J, Barth AL. Somatostatin-expressing neurons in cortical networks. Nat Rev Neurosci. 2016; 17:401–409. [PubMed: 27225074]

47. Murphy SC, Palmer LM, Nyffeler T, Muri RM, Larkum ME. Transcranial magnetic stimulation (TMS) inhibits cortical dendrites. Elife. 2016; 5:e13598. [PubMed: 26988796]

48. Lin LC, Sibille E. Reduced brain somatostatin in mood disorders: a common pathophysiological substrate and drug target? Front Pharmacol. 2013; 4:110. [PubMed: 24058344]

49. Hunt RF, Girskis KM, Rubenstein JL, Alvarez-Buylla A, Baraban SC. GABA progenitors grafted into the adult epileptic brain control seizures and abnormal behavior. Nature Neuroscience. 2013; 16:692-+. [PubMed: 23644485]

50. Dobolyi A, et al. Receptors of Peptides as Therapeutic Targets in Epilepsy Research. Current medicinal chemistry. 2014; 21:764–787. [PubMed: 24251562]

Methods-only References

51. Yang G, Pan F, Chang PC, Gooden F, Gan WB. Transcranial two-photon imaging of synaptic structures in the cortex of awake head-restrained mice. Methods Mol Biol. 2013; 1010:35–43. [PubMed: 23754217]

52. Dana H, et al. Thy1-GCaMP6 transgenic mice for neuronal population imaging in vivo. PLoS One. 2014; 9:e108697. [PubMed: 25250714]

53. Chen TW, et al. Ultrasensitive fluorescent proteins for imaging neuronal activity. Nature. 2013; 499:295–300. [PubMed: 23868258]

54. Chagnacamital Y, Luhmann HJ, Prince DA. Burst Generating and Regular Spiking Layer-5 Pyramidal Neurons of Rat Neocortex Have Different Morphological Features. Journal of Comparative Neurology. 1990; 296:598–613. [PubMed: 2358553]

55. Agmon A, Connors BW. Correlation between Intrinsic Firing Patterns and Thalamocortical Synaptic Responses of Neurons in Mouse Barrel Cortex. Journal of Neuroscience. 1992; 12:319–329. [PubMed: 1729440]

56. Smith SL, Smith IT, Branco T, Hausser M. Dendritic spikes enhance stimulus selectivity in cortical neurons in vivo. Nature. 2013; 503:115–120. [PubMed: 24162850]
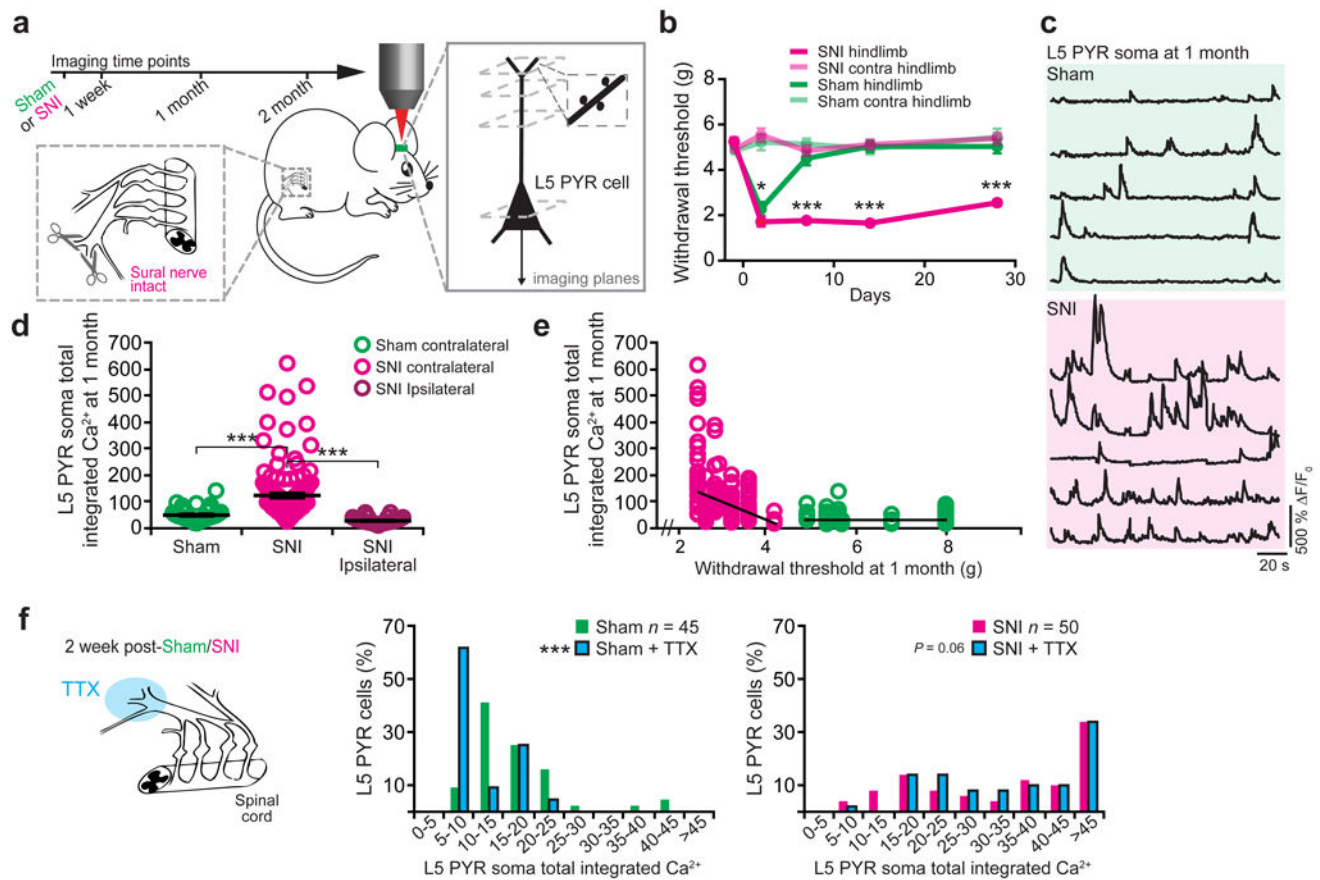
Figure 1. Elevated L5 pyramidal somatic Ca²⁺ activity in the S1 after peripheral nerve injury
(**a**) Schematic of spared nerve injury (SNI) and two-photon Ca²⁺ imaging timeline in the primary somatosensory cortex. Imaging was performed at different cortical depths (dashed boxes) from pial surface in awake, head-restrained mice expressing GCaMP6s in L5 pyramidal (PYR) neurons. (**b**) Measures of hind limb paw withdrawal threshold before and after SNI ($n = 17$ mice) and Sham operations ($n = 12$ mice) (2 d: $P = 0.025$; 7 d: $P < 0.001$; 14 d: $P < 0.001$; 31 d: $P < 0.001$, two-way ANOVA followed by Tukey's test). (**c**) Fluorescence traces of representative L5 PYR soma expressing GCaMP6s in SNI/Sham mice at 1 month post-surgery. (**d**) Average total integrated Ca²⁺ activity over 2.5 min in L5 PYR 1 month after surgery (SNI: 116.2 ± 8.5 F, $n = 141$ cells from 5 mice; sham: 41.6 ± 2.9 F, $n = 59$ cells from 5 mice; $t_{198} = 5.581$, $P < 0.001$, unpaired t test; SNI ipsilateral: 20.2 ± 1.0 F, $n = 106$ cells, $t_{245} = 9.694$, $P < 0.001$, unpaired t test). (**e**) L5 PYR soma Ca²⁺ activity at 1 month correlates with the hind limb paw withdrawal threshold in SNI mice (Pearson $r = -0.33$, $P < 0.001$), but not in Sham mice (Pearson $r = 0.046$, $P = 0.609$). (**f**) L5 PYR soma total integrated Ca²⁺ activity before (SNI: 40.3 ± 3.6 F, $n = 50$ cells from 2 mice; Sham: 17.1 ± 1.2 F, $n = 45$ cells) and after local application of TTX to sciatic nerve (SNI: 41.9 ± 3.7 F, $t_{49} = 1.928$, $P = 0.06$, paired t test; Sham: 11.6 ± 0.9 F, $t_{44} = 12.08$, $P < 0.001$, paired t test) at 2 weeks post-Sham/SNI. Data are presented as means $\pm$ s.e.m. *$P < 0.05$, ***$P < 0.001$. (**c**) Representative traces from experiments carried out on at least 5 animals per group.
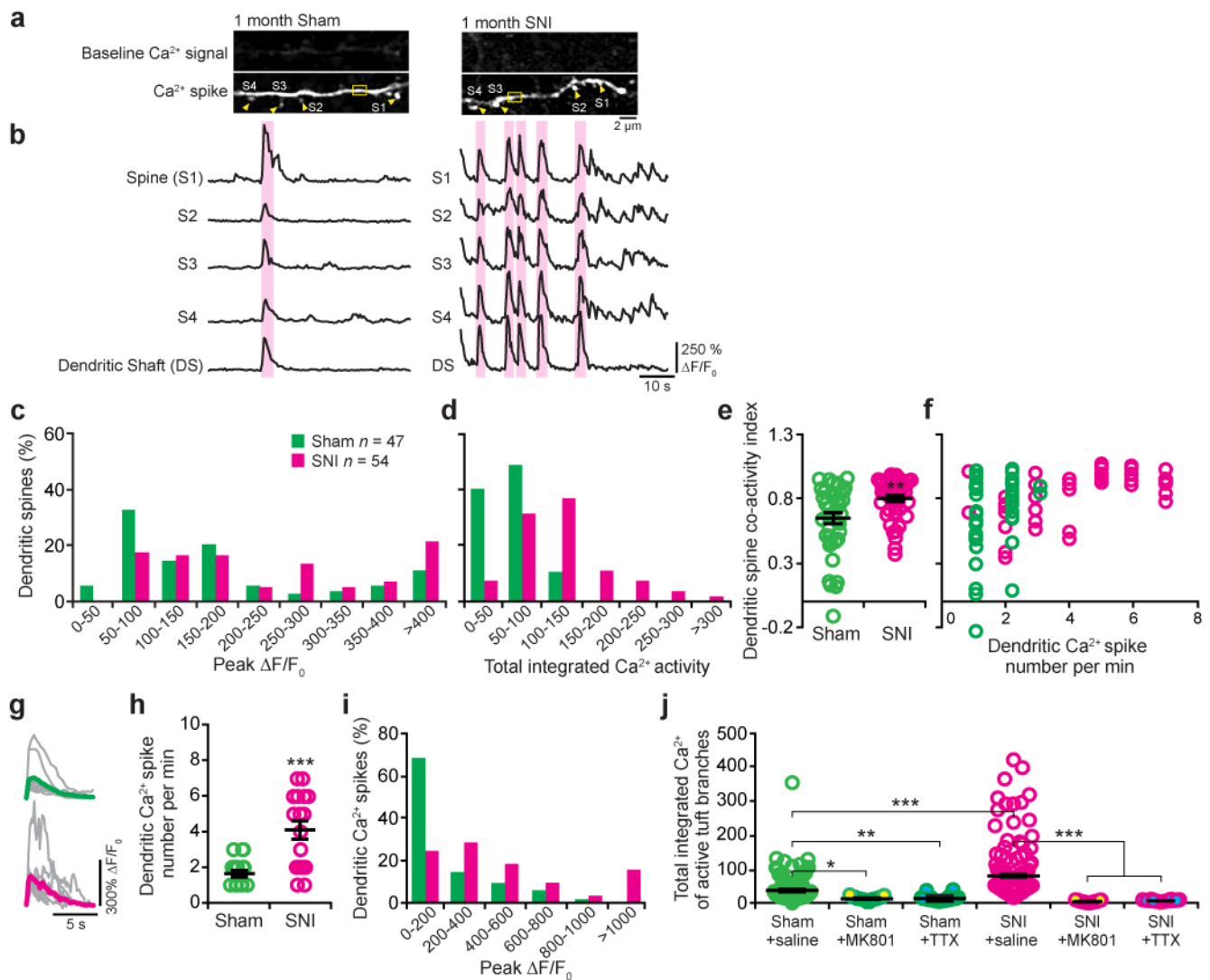
Figure 2. Enhanced dendritic spine and branch activities in the S1 of neuropathic pain mice

(**a**) Representative two-photon images of active, apical tuft dendrites of L5 PYR neurons expressing GCaMP6s in SNI/Sham mice at 1 month post-surgery. Arrowheads point to spine heads measured. (**b**) Fluorescence traces of dendritic spines and adjacent shaft show increased Ca^{2+} transients in spines and shaft of SNI as compared to Sham mice. Light magenta bars indicate Ca^{2+} elevations in both spine heads and shaft, indicating Ca^{2+} spike generation. (**c**) Distribution of peak Ca^{2+} amplitude of dendritic spines over 1 minute (SNI: 282 ± 21 peak $\Delta F/F_0$, $n = 54$ spines from 3 mice; Sham: 183 ± 13 peak $\Delta F/F_0$, $n = 47$ spines from 3 mice; $t_{231} = 4.116$, $P < 0.001$). (**d**) Distribution of average total integrated Ca^{2+} activity of dendritic spines over 1 minute (SNI 125 ± 8.2 ΔF, Sham 66.5 ± 4.1 ΔF, $t_{99} = 6.078$, $P < 0.001$). (**e**) Average spine co-activity index in SNI/Sham mice (SNI 0.8 ± 0.02, $n = 43$ spines; Sham 0.63 ± 0.04, $n = 40$ spines; $t_{81} = 3.368$, $P < 0.01$). (**f**) In both SNI and Sham mice, L5 cell spine co-activity correlates with the generation of apical tuft dendritic Ca^{2+} spike (SNI: Pearson $r = 0.54$, $P < 0.001$; Sham: Pearson $r = 0.33$, $P < 0.05$). (**g**) Fast-scanning of individual tuft Ca^{2+} events in SNI (rise time, 0.7 ± 0.2 s, decay time, 4.8 ± 1.5 s,

$n = 11$ dendrites) and Sham mice (rise time, 0.6 ± 0.1 s, decay time, 4.5 ± 0.5 s, $n = 9$ dendrites). Average trace shown as magenta for SNI and green for Sham. (**h**) Average number of dendritic Ca^{2+} spikes per minute recording on dendrites (SNI, 4.1 ± 0.5 transients/min; Sham, 1.7 ± 0.2 transients/min; $t_{32} = 4.509$, $P < 0.001$). (**i**) Distribution of peak Ca^{2+} amplitudes of dendritic Ca^{2+} spikes (SNI, 534 ± 38.5 F/F_0, $n = 147$ spikes from 5 mice; Sham, 192 ± 19.4 F/F_0, $n = 117$ spikes from 5 mice, $t_{262} = 7.393$, $P < 0.001$). (**j**) Average total integrated Ca^{2+} activity detected with GCaMP6s over 2.5 min in active tuft apical dendrites (SNI, 80.2 ± 6.6 F, $n = 147$ dendrites; Sham, 37.0 ± 4.0 F, $n = 117$ dendrites, $t_{408} = 6.613$, $P < 0.001$). Local application of either MK801 or TTX to L1 in SNI/ Sham mice at 1 month post-surgery (SNI+MK801: 4.0 ± 0.6 F, $n = 30$ dendrites from 2 mice, $t_{408} = 7.22$, $P < 0.001$; Sham+MK801: 8.4 ± 1.2 F, $n = 38$ dendrites from 2 mice, $t_{408} = 2.918$, $P = 0.011$; SNI+TTX: 6.6 ± 0.7 F, $n = 37$ dendrites from 4 mice, $t_{408} = 7.593$, $P < 0.0001$; Sham+TTX: 5.6 ± 0.5 F, $n = 45$ from 2 mice, $t_{408} = 3.402$, $P = 0.0022$). Data are presented as means $\pm$ s.e.m. *$P < 0.05$, **$P < 0.01$, ***$P < 0.001$, unpaired t test in (**c-e, h, i**), two-way ANOVA followed by Bonferroni's test in (**j**). (**a-b**) Representative images and traces from experiments carried out on at least 3 animals per group.
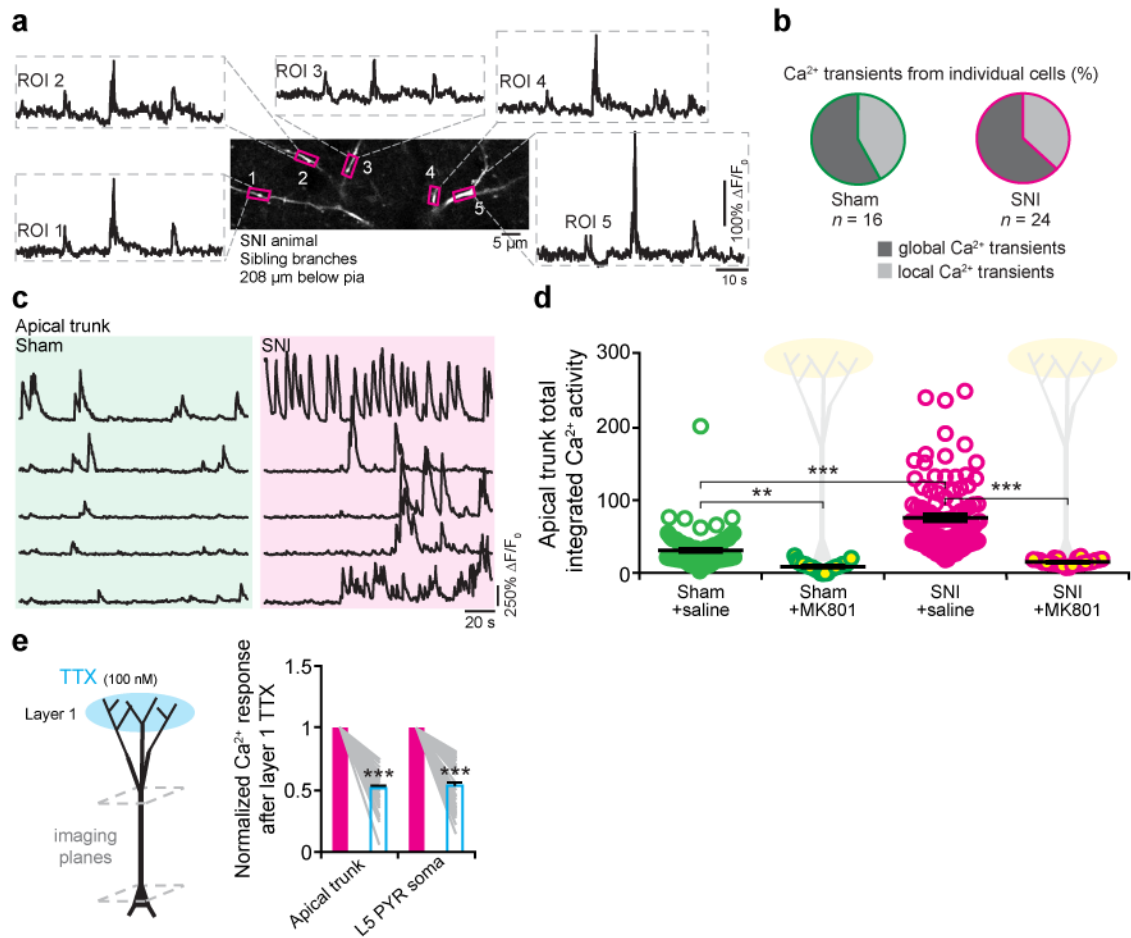
Figure 3. Elevated dendritic Ca^{2+} spike generation in apical tuft branches and trunks of L5 pyramidal neurons in the S1 of neuropathic pain mice

(**a**) Two-dimensional projection of multiple sibling branches from an individual L5 PYR neuron in SNI mice. Five regions-of-interests (ROIs) (magenta box) corresponding to different dendritic branches were analyzed. All ROIs generated multiple Ca^{2+} transients during recording. (**b**) Percentages of local or global Ca^{2+} spikes observed on sibling branches from individual PYR neurons (SNI, 9.8 ± 1.2 transients/min, $n = 24$ cells from 3 mice; Sham, 4.8 ± 1.0 transients/min, $n = 16$ cells from 3 mice). Ca^{2+} events were analyzed over 2.5 min. (**c**) Fluorescence traces of apical dendritic trunks imaged at ~300 μm below the pial in SNI/Sham mice. (**d**) Average total integrated Ca^{2+} activity over 2.5 min in apical trunk (SNI, 77.2 ± 4.8 F, $n = 102$ trunks from 5 mice; Sham, 32.9 ± 2.3 F, $n = 103$ trunks from 5 mice; $t_{255} = 9.34$, $P < 0.001$). Local application of MK801 in SNI (16.7 ± 0.8 F, $n = 26$ trunks from 2 mice, $t_{255} = 8.111$, $P < 0.001$, two-way ANOVA followed by Bonferroni's test) and Sham mice (8.3 ± 0.9 F, $n = 28$ trunks from 2 mice, $t_{255} = 3.4$, $P = 0.0016$). (**e**) TTX locally applied to L1 (blue shaded circle) significantly reduced Ca^{2+} activity in apical trunk and L5 soma (noted by grey dashed lines) in SNI mice (before TTX: 1; trunk after TTX: 0.51 ± 0.02, $n = 50$ trunks, $t_{49} = 23.77$, $P < 0.001$, paired t test; soma after TTX: 0.53 ± 0.03, $n = 54$ cells, $t_{53} = 17.19$, $P < 0.001$; trunks and cells not related to same cells). Data
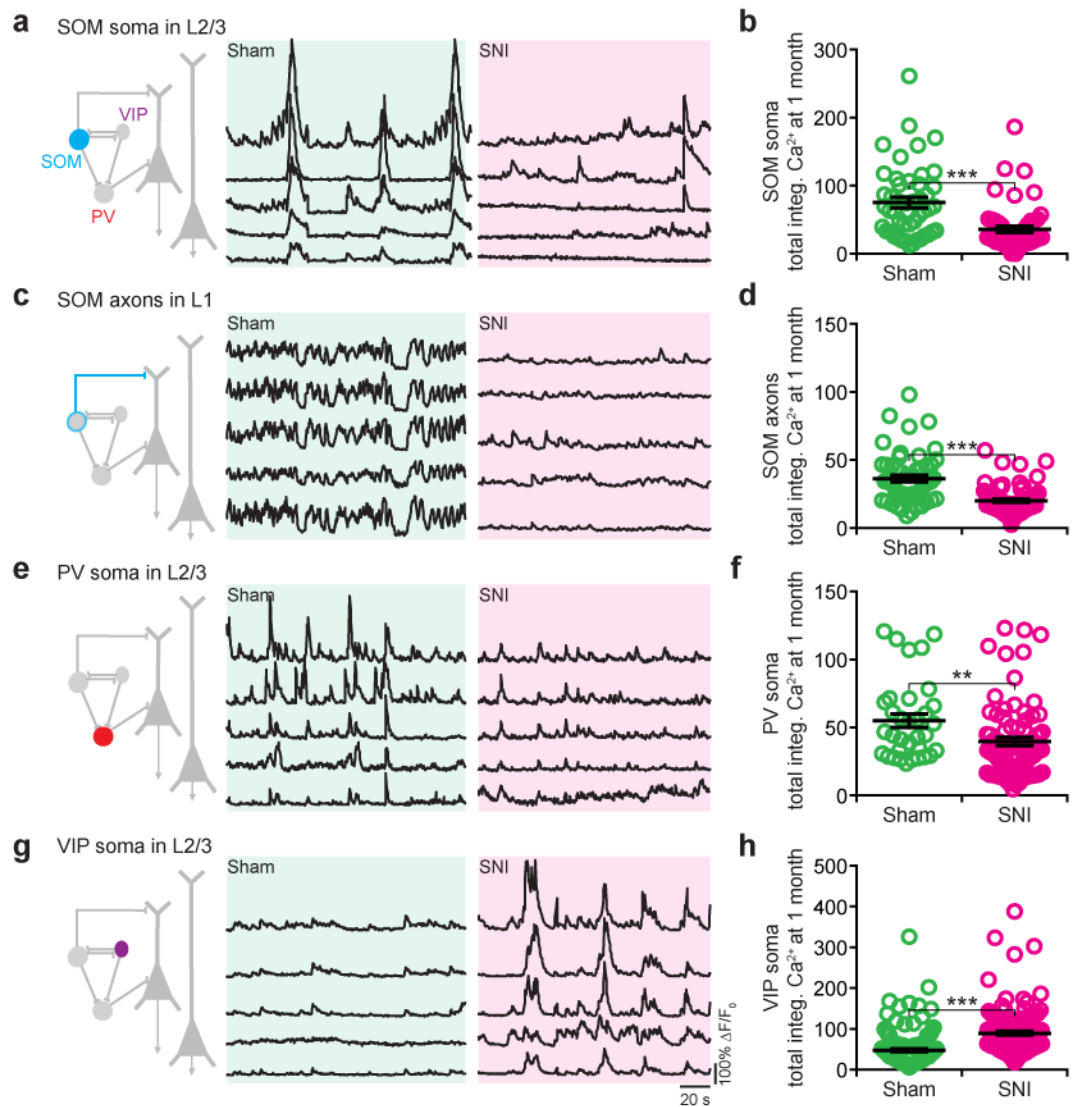
are presented as means ± s.e.m. **P < 0.01, ***P < 0.001. (**a,c**) Representative traces from experiments carried out on at least 3 animals per group.

Figure 4. Alterations in inhibitory neuronal Ca^{2+} activity in the S1 of neuropathic pain mice
(**a–d**) Cartoon (left of traces) depicting cortical interneuron subtype imaged with GCaMP6s (highlighted by color). Representative fluorescence traces (right) and average total integrated Ca^{2+} activity over 2.5 min recordings of L2/3 SOM-positive somata and axon fibers expressing GCaMP6s in SNI/Sham mice at 1 month (soma: SNI 36.0 ± 4.7 F, $n = 117$ cells from 4 mice, Sham 75.2 ± 7.7 F, $n = 68$ cells from 3 mice; $t_{183} = 6.825$, $P < 0.001$; axon: SNI 19.1 ± 1.1 F, $n = 80$ fibers from 4 mice, Sham 42.5 ± 3.1 F, $n = 61$ fibers from 3 mice; $t_{139} = 9.008$, $P < 0.001$). (**e–h**) Representative fluorescence traces and quantification of average total integrated Ca^{2+} activity of L2/3 PV-positive (**e–f**; SNI, 40.0 ± 3.0 F, $n = 81$ cells from 3 mice; Sham, 55.5 ± 5.1 F, $n = 66$ cells from 3 mice; $t_{145} = 2.707$, $P < 0.01$) and L2/3 VIP-positive (**g–h**; SNI, 90.0 ± 5.0 F, $n = 133$ cells from 4 mice; Sham, 47.9 ± 3.6 F, $n = 144$ cells from 4 mice; $t_{275} = 6.899$, $P < 0.001$) neurons at 1 month. Data are presented as means $\pm$ s.e.m. **$P < 0.01$, ***$P < 0.001$, unpaired t test. (**a, c, e, g**) Representative traces from experiments carried out on at least 3 animals per group.
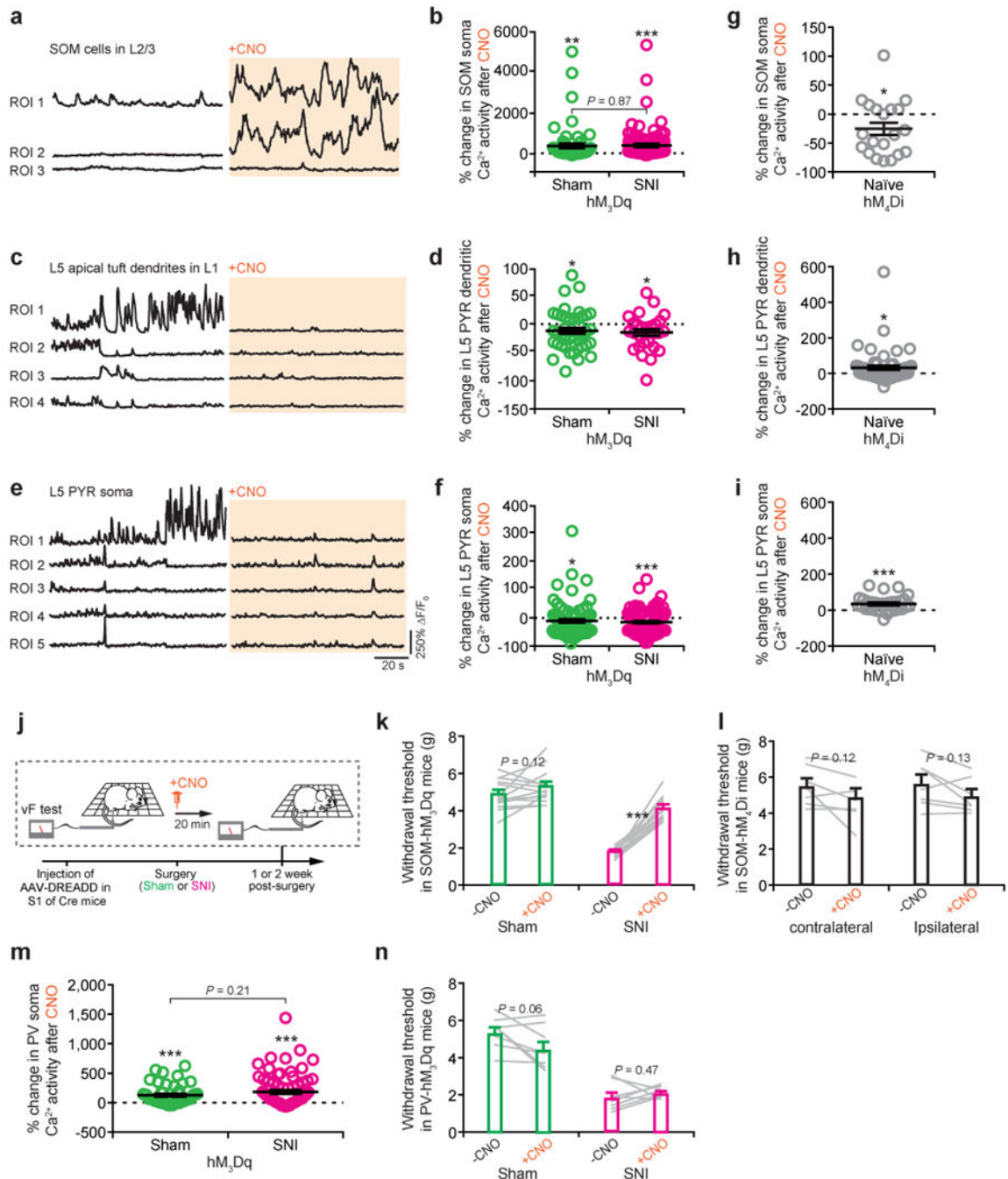
Figure 5. Acute activation of SOM neurons in the S1 reduces L5 pyramidal neuron activity in neuropathic pain mice

(**a**) Representative fluorescence traces of SOM neurons expressing GCaMP6s/hM$_3$Dq-mcherry before and after CNO injection in SNI mice. (**b**) Percent change in average Ca^{2+} activity of SOM somata over 2.5 min following CNO injection in SNI (382 ± 78%, n = 93 cells from 4 mice) and Sham mice (361 ± 114%, n = 61 cells from 5 mice). SOM Ca^{2+} activity significantly increased from baseline activity upon CNO injection (SNI: t_{92} = 4.912, P < 0.001; Sham: t_{60} = 3.168, P < 0.01, paired t test). No significant difference was found

between SNI and Sham mice after CNO injection ($t_{152} = 0.163$, $P = 0.87$, unpaired t test). (**c**) Representative fluorescence traces of apical dendrites of L5 PYR neurons expressing GCaMP6 before and after CNO injection to activate SOM/hM$_3$Dq-positive neurons in SNI mice. (**d**) Dendritic Ca^{2+} activity of L5 PYR neurons following CNO injection in SNI (-14.5 ± 5.5%, $n = 29$ dendrites from 3 mice; $t_{28} = 2.522$, $P = 0.0176$, paired t test) and Sham mice (-11.5 ± 5.3%, $n = 43$ dendrites from 4 mice; $t_{42} = 2.149$, $P = 0.0374$). (**e**) Representative fluorescence traces of L5 PYR neuron somata expressing GCaMP6s before and after CNO injection to activate SOM/hM$_3$Dq-positive neurons in SNI mice. (**f**) L5 PYR somatic Ca^{2+} activity following CNO injection in SNI (-17.9 ± 4.0%, $n = 94$ cells; $t_{93} = 4.449$, $P < 0.001$, paired t test) and Sham mice (-13.7 ± 5.9 %, $n = 87$ cells; $t_{86} = 2.310$, $P < 0.05$). (**g**) Percent change in average total integrated Ca^{2+} activity of SOM somata following CNO injection in naïve mice infected with hM$_4$Di. SOM Ca^{2+} activity significantly decreased from baseline activity upon CNO injection (-25.4 ± 10.6%, $n = 20$ cells from 2 mice, $t_{19} = 2.381$, $P = 0.03$). (**h, i**) Inactivating SOM cells with hM$_4$Di exacerbated Ca^{2+} activity of L5 PYR dendrites (**h**, % change in L5 dendritic Ca^{2+} activity after CNO: Sham: 32.9 ± 14.1 %, $n = 60$ dendrites, $t_{59} = 2.35$, $P = 0.02$, paired t test; SNI: 21.6 ± 6.6 %, $n = 40$ dendrite, $t_{39} = 3.195$, $P = 0.003$, paired t test) and somata (**i**, % change in L5 PYR somata Ca^{2+} activity after CNO: Sham: 31.7 ± 5.0%, $n = 60$ soma, $t_{59} = 6.289$, $P < 0.001$, paired t test; SNI: 13.9 ± 6.5%, $n = 52$ soma, $t_{51} = 2.126$, $P < 0.05$, paired t test) in naïve mice. (**j**) Cartoon depicting design for determining mechanical allodynia before and after CNO-induced SOM cell activation or inactivation. Thresholds measured before and 20 min after CNO injection in SNI/Sham mice. (**k**) Withdrawal threshold after SOM activation by CNO in SNI (before CNO: 1.7 ± 0.1 g, after 20-min CNO: 4.0 ± 0.2 g, $n = 14$ mice; $t_{13} = 12.97$, $P < 0.001$, paired t test) and Sham mice (before CNO: 4.8 ± 0.4 g, after 20-min CNO: 5.2 ± 0.2 g, $n = 14$ mice; $t_{13} = 1.685$, $P = 0.12$, paired t test). (**l**) Withdrawal threshold before and after CNO injection in naïve mice infected with hM$_4$Di. Inactivating SOM cells had no significant effects on the animals' withdraw threshold (contralateral paw: $P = 0.12$, paired t test; ipsilateral paw: $P = 0.13$, paired t test). (**m**) Percent change in average total integrated Ca^{2+} activity of PV somata following CNO injection in SNI (185 ± 29.7%, $n = 81$ cells from 3 mice) and Sham mice (131 ± 24.5%, $n = 48$ cells from 3 mice). PV Ca^{2+} activity significantly increased from baseline activity upon CNO injection (SNI: $t_{80} = 6.243$, $P < 0.001$; Sham: $t_{47} = 5.339$, $P < 0.001$, paired t test). No significant difference was found between SNI and Sham mice after CNO injection ($t_{127} = 1.262$, $P = 0.21$, unpaired t test). (**n**) Withdrawal threshold after PV activation by CNO in Sham (before CNO: 5.4 ± 0.3 g, after 20-min CNO: 4.5 ± 0.4 g, $n = 8$ mice; $t_7 = 2.305$, $P = 0.06$, paired t test) and SNI mice (before CNO: 1.9 ± 0.3 g, after 20-min CNO: 2.1 ± 0.1 g, $n = 8$ mice; $t_7 = 0.7693$, $P = 0.47$, paired t test). Data are presented as means ± s.e.m. *$P < 0.05$. **$P < 0.01$, ***$P < 0.001$. (**a, c, e**) Representative traces from experiments carried out on at least 3 animals per group.
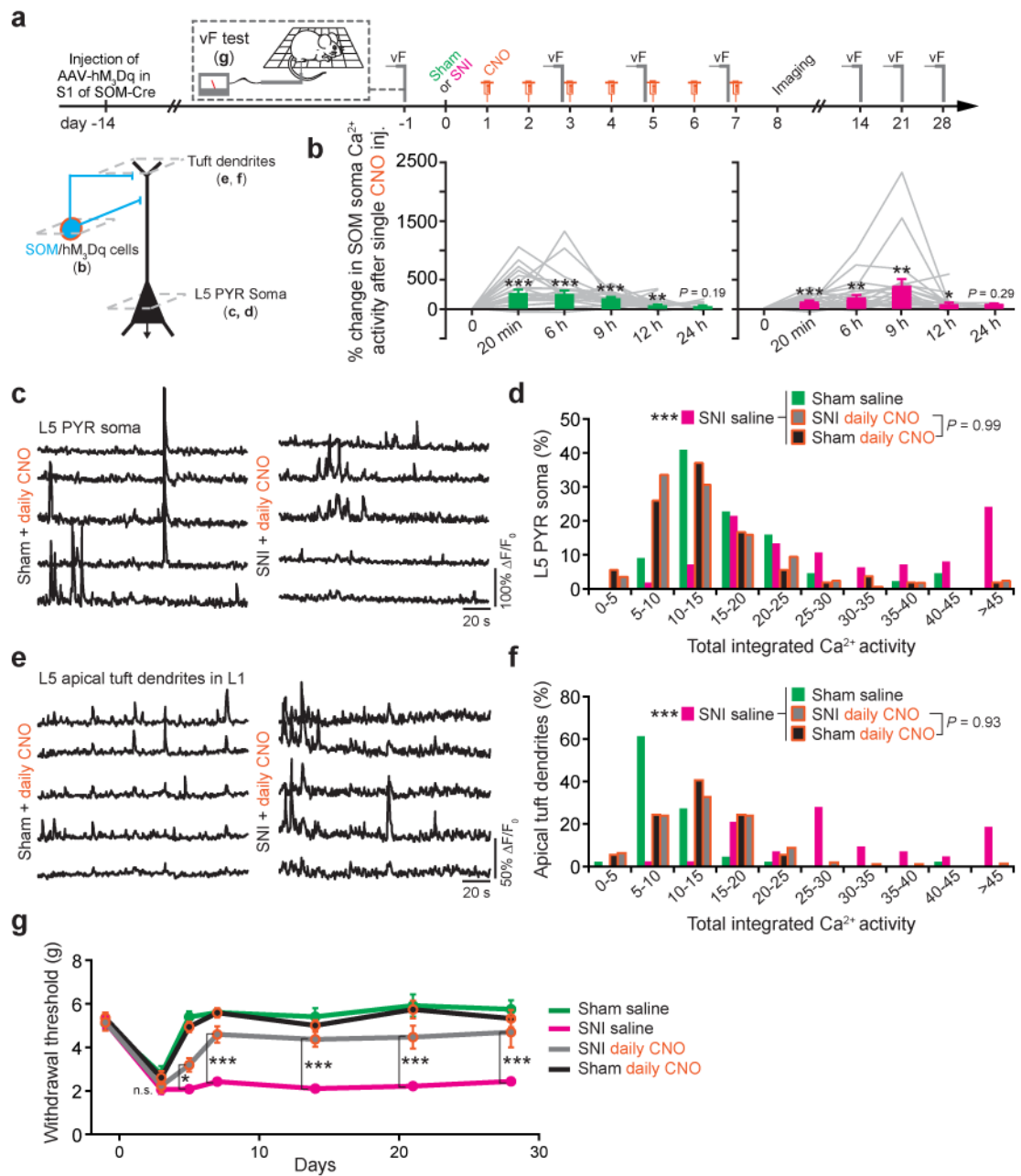
Figure 6. Daily activation of SOM neurons following perpherial nerve injury prevents the development of neuropathic pain

(**a**) Top panel, experimental design for daily activation of SOM neurons following SNI or sham surgeries (CNO, orange syringe; vF, von Frey). For control, SNI and sham mice received saline injections. Bottom panel, cartoon of two-photon imaging planes corresponding to SOM somata (**b**), pyramidal somata (**c,d**) and pyramidal tuft dendrites (**e,f**). (**b**) Percent change in average total integrated Ca^{2+} activity of SOM somata over 2.5 min following single CNO injection in SNI ($n = 23$ cells from 2 mice) and Sham mice ($n = 26$ cells from 2 mice). CNO injection significantly increased from baseline activity of SOM cells for at least 12 h ($P < 0.001$) but not 24 h (Sham, $P = 0.19$; SNI, $P = 0.29$). (**c**)

Fluorescence traces of L5 PYR neuron somata expressing GCaMP6s after 1-week of daily CNO activation of SOM cells in SNI/Sham mice. (**d**) Average total integrated Ca^{2+} activity over 2.5 min recording of L5 PYR somata following 1-week daily SOM activation in SNI (14.4 ± 0.7 F, $n = 170$ soma from 5 mice) and Sham mice (14.4 ± 1.2 F, $n = 54$ soma from 5 mice). No significant difference between SNI and Sham mice treated with CNO ($t_{377} = 7.171$, $P = 0.99$). (**e**) Fluorescence traces of L5 apical tuft dendrites expressing GCaMP6s after 1-week of daily SOM activation in SNI and Sham mice. (**f**) Average total integrated Ca^{2+} activity over 2.5 min recording of L5 dendrites following 1-week daily SOM activation in SNI (14.1 ± 0.7 F, $n = 159$ dendrites from 5 mice) and Sham mice (12.9 ± 0.8 F, $n = 37$ dendrites from 5 mice). No significant difference between SNI and Sham mice treated with CNO ($t_{279} = 0.7357$, $P = 0.9251$). (**g**) Withdrawal threshold under various conditions. Daily SOM activation significantly increased withdrawal threshold in SNI mice as compared to SNI mice with IP saline ($P < 0.05$ at day 5 and $P < 0.001$ at day 7, 14, 21, and 28). Data are presented as means $\pm$ s.e.m. *$P < 0.05$, **$P < 0.01$, ***$P < 0.001$, paired t test in (**b**), two-way ANOVA followed by Bonferroni's test in (**d, f**), and Tukey's test in (**g**). (**c, e**) Representative traces from experiments carried out on at least 3 animals per group.